# Azobenzene-Based Low-Potential Anolyte for Nonaqueous Organic Redox Flow Batteries

Xiao Wang[+], Jingchao Chai[+], Amir Lashgari, and Jianbing Jimmy Jiang*[a]

Redox flow batteries (RFBs) using organic materials in organic solvents are particularly promising because of the diversity of organic materials and the wide redox-innocent window of organic solvents, yet the further development of this type of RFB has been hindered by the lack of suitable anolyte materials with high potentials, solubility, and stability. Herein, we examine the physical and electrochemical properties of azobenzene (**AzoPh**) compounds and investigate their degradation mechanism in nonaqueous organic RFB. The azobenzene displayed two-electron activity at −1.69 and −2.20 V vs. Ag/Ag$^+$. Paired with a well-established PEGylated phenothiazine (**PEG3-PTZ** ) catholyte, the battery presents a high theoretical cell voltage of 2.08 V. The azobenzene-based RFB displays a capacity retention of 93.3% over 50 cycles with an average fade rate of 0.13% per cycle. The capacity decay mechanism was probed by proton nuclear magnetic resonance spectroscopy, cyclic voltammetry, and high-resolution mass spectrometry, and revealed proton-assisted degradation mechanisms.

## 1. Introduction

The ever-increasing energy demand and growing environmental concerns prompted the use of clean energy from renewable sources, such as solar, wind, and tide. The inherent intermittence of these energy sources requires the use of high-performance energy storage systems, such as supercapacitors, lithium ion batteries, and other rechargeable metal batteries.[1] As a reliable large-scale electricity storage technology, redox flow batteries (RFBs) can be deployed to integrate intermittent energy sources into the smart grids.[2] In RFBs, the redox-active materials are dissolved in liquid electrolytes (termed anolyte and catholyte) and stored in external reservoirs. During charge/discharge processes, the anolyte and catholyte solutions are pumped through an electrochemical cell where energy conversion occurs.[3] Owning to this unique configuration, RFBs possess promising features, such as high safety, long lifetime, and independent control over energy capacity and power density.[4]

While remarkable progress was made in the past decades in terms of cyclability and cost control,[2c,d,5] the low energy density of traditional RFBs still limits the wide application of RFBs. Organic compounds as redox-active materials in RFBs have attracted enormous attention owing to the multi-electron activity, structural tunability, and remarkable room for lowering cost.[6] The energy density of RFBs is determined by the number of electrons transferred for each half reaction, redox potentials, and the electrolyte concentration. The effective strategies to enhance energy density including (1) increasing the concentration of redox-active materials; (2) extending the redox potentials of battery half reactions; and (3) increasing the number of electrons transferred in the half reactions.[6–7] Although effective methods have been developed to enable aqueous RFBs for relatively high voltage,[8] the voltage of most aqueous RFBs is still limited by the narrow electrochemical window of water.[9] Therefore, nonaqueous electrolyte with a wider electrochemical window (>4 V)[10] is employed to broaden the electrochemical window.[11] Several catholyte materials with high positive potential (up to 1.3 V vs. Fc/Fc$^+$), such as cyclopropenium,[12] 2,2,6,6-tetramethylpiperidine-1-oxyl,[13] phenothiazine (**PTZ**),[11a,12b,14] have been investigated and applied in nonaqueous electrolyte systems. The anolyte materials, such as viologens,[4b,15] pyridinium,[16] fluorenone,[17] and anthraquinone,[18] possess redox potentials ranging from −0.8 to −2 V vs. Fc/Fc$^+$. Despite several promising reports on novel anolyte systems,[19] the further advancement of anolyte materials is limited by insufficient stability, tedious synthesis, or unidentified degradation mechanism, necessitating the fundamental investigation on possible surrogates with superior properties.

As a family of long-studied redox- and photo-responsive compounds, azobenzene (**AzoPh**) and its derivatives demonstrate fascinating properties on photo-switches and dye material.[20] Very recently, Wang *et al.* investigated the electrochemical behavior and successfully applied **AzoPh** in lithium-, sodium-, and potassium-ion batteries.[21] During the course of this work, Yu *et al.* reported **AzoPh** at high concentration (1 M) in nonaqueous RFB.[22] Even at extreme negative potential at −2.20 V vs. Ag/Ag$^+$, azo-group compounds upkeep satisfactory cyclability in various batteries, which indicates its excellent stability under different electrochemical conditions.[21a–c] In view of these characteristics, **AzoPh** has considerable prospects for high-voltage nonaqueous RFB applications.

Here we report a nonaqueous organic RFB based on **AzoPh** as the anolyte, with a primary focus on the elucidation of degradation mechanism and the feasibility of the second

[a] X. Wang,[+] Dr. J. Chai,[+] Dr. A. Lashgari, Prof. J. J. Jiang
Department of Chemistry
University of Cincinnati
P.O. Box 210172, Cincinnati,45221-0172, Ohio, United States
E-mail: jianbing.jiang@uc.edu
[+] These authors contributed equally to this work.

Supporting information for this article is available on the WWW under https://doi.org/10.1002/celc.202001035

electron utilization. The redox reaction of **AzoPh** occurs on the azo (N=N) unit and undergoes two one-electron processes in nonaqueous electrolytes. When combined with PEGylated phenothiazine (**PEG3-PTZ**), the battery displays a potential of 2.59 V. The degradation mechanism was also elucidated by a combination of tools of proton nuclear magnetic resonance spectroscopy ($^1$H NMR), cyclic voltammetry (CV), and high-resolution mass spectrometry (HR-MS).

## 2. Results and Discussion

### 2.1. Electrochemical Properties

The electrochemical study of **AzoPh** starts with CV measurements. Since the electrochemical behavior is highly dependent on the electrolyte systems,[8a,23] such as supporting electrolyte and solvent,[16a,24] several different electrolyte systems (Figure 1a and Figure S1) were studied, including different combinations of several most commonly used supporting electrolytes, namely lithium bis(trifluoromethanesulfonyl)imide (LiTFSI), tetrabutylammonium hexafluorophosphate ($TBAPF_6$) and Lithium hexafluorophosphate ($LiPF_6$), and solvents, namely acetonitrile (MeCN) and propylene carbonate (PC) and dimethoxyethane (DME). Instead of forming a weakly bound complex, lithium ion associates with the reduced **AzoPh** tightly to form stable lithiated **AzoPh**,[24] resulting in inferior redox reversibility (green and blue traces in Figure 1a). **AzoPh** displayed instability in $TBAPF_6$/PC at positive potential, and an anodic peak at −0.3 V vs. $Ag/Ag^+$ was observed. **AzoPh** delivered a reversible redox couple at −1.69 V vs. $Ag/Ag^+$ in 0.1 M $TBAPF_6$/MeCN (red trace in Figure 1a). Remarkably, when the cathodic cut-off voltage of CV is extended to −2.6 V vs. $Ag/Ag^+$, **AzoPh** displays two redox peaks at −1.69 and −2.20 V vs. $Ag/Ag^+$ (Figure 1b), indicating two-electron activity (**AzoPh**$^-$/**AzoPh**$^0$ and **AzoPh**$^{2-}$/**AzoPh**$^-$).[21b,25]

The **PEG3-PTZ** catholyte with three ethylene glycol units (PEG3) is synthesized following a reported procedure from our group[26] (Figure S2 and Scheme 1). Compared with **PEG12-PTZ** with 12 PEG units in our previous study, **PEG3-PTZ** has higher neat concentration (3.39 M vs. 1.72 M)[26b] for higher energy density. Odom *et al.* conducted in-depth research on phenothiazine compounds and demonstrated promising performance in organic RFBs.[11a,12b,14] The combination of **AzoPh** and **PEG3-PTZ** presents a theoretical voltage of 2.08 V for one-electron utilization of **AzoPh** and 2.59 V for two-electron utilization (Figure 1b and Figure S3).

A rotating disk electrode (RDE) study was performed to probe the redox kinetics of **AzoPh** and **PEG3-PTZ** (Figure 2a). The limiting current has a significant linear correlation with the square root of the angular speed (Figure 2b). According to the Lévich equation (Equation S1 in Supporting Information),[2c,27] the diffusion coefficients of the redox pairs of **AzoPh**$^-$/**AzoPh**$^0$, **AzoPh**$^2$/**AzoPh**$^-$, and **PEG3-PTZ**$^0$/**PEG3-PTZ**$^+$ were determined to be $2.15\times10^{-5}$, $6.82\times10^{-5}$, and $5.49\times10^{-5}$ cm$^2$/s, respectively. These values are comparable with those of the reported materials in RFBs.[10,28] Furthermore, the kinetic rate constant ($k_0$)

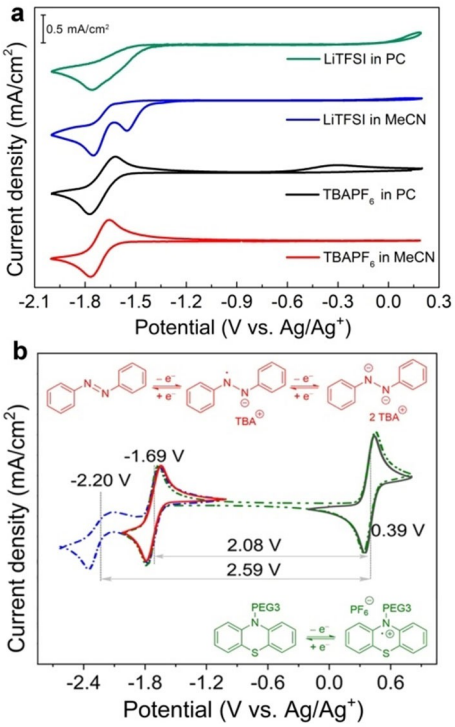


**Figure 1.** a) Cyclic voltammograms of 5 mM **AzoPh** in different electrolyte systems. b) Redox reactions and cyclic voltammograms of anolyte and catholyte at 5 mM concentrations in 0.1 M $TBAPF_6$/MeCN using glassy carbon as working electrode at a scan rate of 50 mV s$^{-1}$.

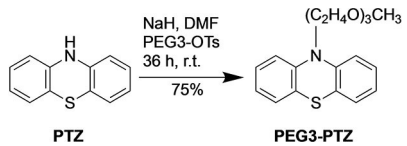


**Scheme 1.** Synthesis of **PEG3-PTZ**.

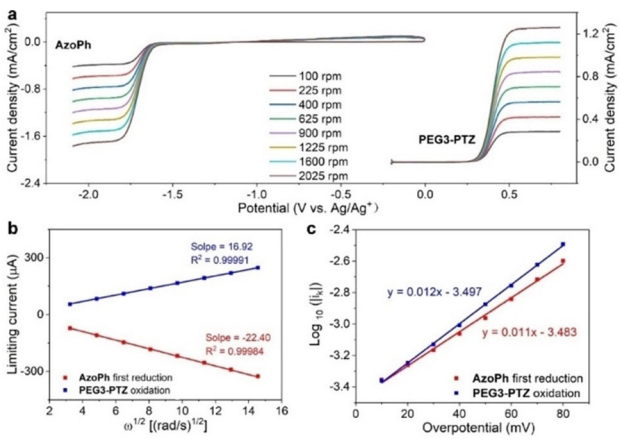


**Figure 2.** a) Linear sweep voltammetry plots of **AzoPh** and **PEG3-PTZ** at different rotation rates of the rotating disk electrode. b) Reduction and oxidation peak current density vs. square root of angular velocity. c) Tafel plot constructed using the current response and overpotentials. Solution: 1 mM **AzoPh** and 1 mM **PEG3-PTZ** in 0.1 M $TBAPF_6$/MeCN.

for quantifying the rate of electric chemical reaction were obtained using the Butler-Volmer equation (Equation S2 in Supporting Information),[2c,5a,29] giving kinetic rate constants of $1.74\times10^{-2}$, $1.68\times10^{-2}$, and $8.90\times10^{-2}$ cm/s for **AzoPh$^{-}$/AzoPh$^{0}$**, **AzoPh$^{2-}$/AzoPh$^{-}$** and **PEG3-PTZ$^{0}$/PEG3-PTZ$^{+}$**, respectively (Figure 2c and Figure S4–5). The kinetics observed are analogous with other reported redox systems.[19c,30] The rapid kinetics of the molecules themselves are the basis to achieve fast electron transfer for high power density.[31]

### 2.2. Battery Performance

A mixed electrolyte of 100-mM AzoPh and 100-mM PEG3-PTZ in 0.5 M $TBAPF_6$/MeCN was used as catholyte (14.4 mL) and anolyte (12 mL) to minimize the interference of crossover of redox-active materials on battery performance analysis. A piece of porous Daramic® 175 separator was utilized in the NAORFBs system. Excess catholyte is used to ensure complete electrochemical reaction of AzoPh in the anolyte side. The open-circuit voltage (OCV) of a RFB is dictated by the state of charge (SOC) and the potential of the redox couples.[2c,32] The OCV of the AzoPh/PEG3-PTZ battery rapidly increases with SOCs ranging from 10% to 30%, and a potential plateau was observed at 2.05 V in the SOC range of 30%~100% (Figure 3a), corresponding to the redox couples of AzoPh$^{-}$/AzoPh$^{0}$ (−1.69 V vs. Ag/Ag$^{+}$) and PEG3-PTZ$^{0}$/PEG3-PTZ$^{+}$(−0.39 V vs. Ag/Ag$^{+}$). The high-frequency area specific resistance (ASR), which mainly reflects the membrane resistance, accounts for 80% of the entire cell polarization ASR (Figure S6). Furthermore, the polarization curves of power density and current density (Figure 3b) present a power density of 129 mW/cm$^2$.

To test the rate performance of **AzoPh/PEG3-PTZ** battery, the battery was subjected to galvanostatic charge and discharge at pre-defined current densities within the potential range of 1.2–2.5 V. At a current density of 20 mA/cm$^2$, the battery presented a discharge capacity of 23.8 mAh, corresponding to 73.9% of the theoretical capacity (32.2 mAh) (Figure 3c, d). At a current density of 50 mA/cm$^2$, the discharge capacity is 15.4 mAh, corresponding to 47.8% of the theoretical capacity (Figure 3c, d). The decreased discharge capacity is caused by increased overpotential from

increased current density. Consequently, the Coulombic efficiencies increased from 70.2% (20 mA/cm$^2$) to 85.7% (50 mA/cm$^2$), which is due to alleviated crossover resulted from shortened cycling time at higher current density. The battery displayed quite consistent energy efficiencies of 59.0%, 60.3%, 58.6%, 54.4% at 20, 30, 40, 50 mA/cm$^2$, respectively. The voltage efficiency decreased from 85.7% at 20 mA/cm$^2$ to 63.6% at 50 mA/cm$^2$ owing to the polarization loss and increased overpotential.[33]

Cyclability is one of the most important metrics for assessing the long-term stability and viability of a flow battery.[6,34] To balance the two important aspects of high capacity utilization and high efficiency, a current density of 40 mA/cm$^2$ was applied for long-cycling studies. A 100-mM **AzoPh/PEG3-PTZ** battery for one-electron utilization was subjected to galvanostatic charge and discharge measurement. The resting time between charging and discharging processes has a great effect on the Coulombic efficiencies owing to the crossover of active materials through the Daramic® separator. The Coulombic efficiencies of the battery with resting times of 15 s and 1 s are 81.2% and 84.2%, respectively (Figure 3e). However, the resting time has little effect on the discharge capacity. At a current density of 40 mA/cm$^2$, the battery delivers a discharge capacity of 17.8 mAh for the first cycle. The **AzoPh/PEG3-PTZ** battery displays a capacity retention of 93.3% over 50 cycles, with an average fade rate of 0.13% per cycle. For cycles 50$^{th}$–80$^{th}$, faster capacity decay was observed and the average fade rate increased to 0.75% per cycle. In addition, more prominent polarization changes in the last 30 cycles (50$^{th}$–80$^{th}$ cycles) were also observed in the charge and discharge curve (Figure 3f), which is presumably due to the accelerated parasitic radical reactions, as discussed below.

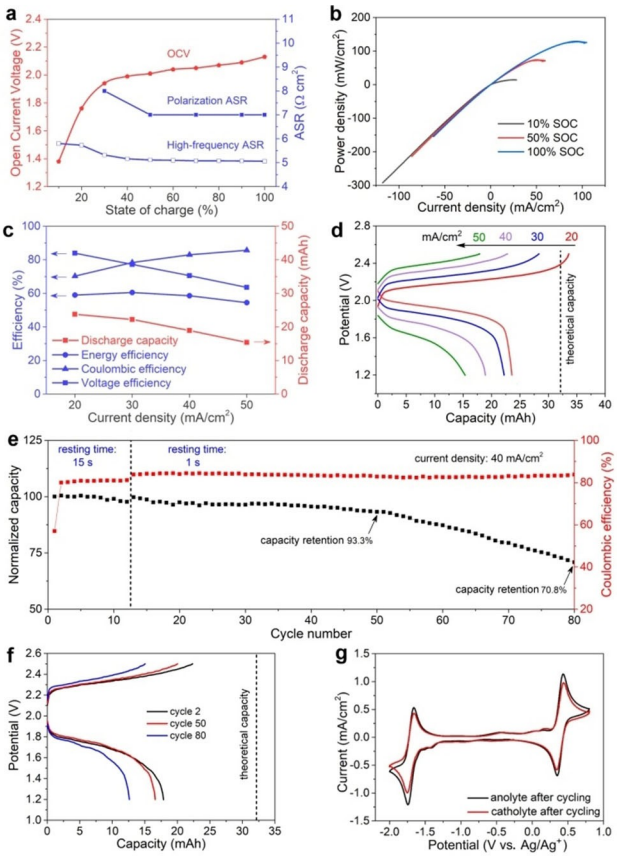


**Figure 3.** Performances of **AzoPh/PEG3-PTZ** battery. a) Open-circuit voltage, high-frequency ASR, and polarization ASR vs. the state of charge (SOC). b) Power density of the battery at varied SOC. c) Coulombic efficiency, energy efficiency, voltage efficiency, and discharge capacity at current densities from 20 to 50 mA/cm$^2$. d) Charge/discharge profiles at different current densities. e) Discharge capacity, coulombic efficiency over 80 cycles at 40 mA/cm$^2$. f) Charge/discharge profiles at varied cycles at a current density of 40 mA/cm$^2$. g) Cyclic voltammograms of anolyte and catholyte after 80 cycles.

### 2.3. Post-cycling Analysis and Possible Degradation Mechanisms

To further understand the degradation mechanism of the **AzoPh/PEG3-PTZ** battery, a series of measurements and analysis of the post-cycling electrolytes were carried out. Given the high reactivity of the azo (N=N) unit toward both reductive and oxidative reactions and the fact that trace water from solvents can have a non-negligible effect on battery performance,[35] we hypothesized that **AzoPh** underwent chemical reactions in the presence of extraneous protons under redox conditions, and generated side products, such as aniline, hydrogenated azobenzene (**H-AzoPh**), and azobenzene oxide (**O-AzoPh**, Figure 4a). To verify this hypothesis, $^1$H NMR of the electrolytes before and after cycling were performed, and compared with the spectra of authentic aniline, **H-AzoPh**, and **O-AzoPh** under the same measurement conditions. After 80 cycles, the **AzoPh** and **PEG3-PTZ** compounds are still the main species in both catholyte and anolyte (Figure S7); however, several non-negligible new peaks were observed in the post-cycling electrolytes (Figure 4b). The $^1$H NMR spectra of the post-cycling anolyte indicate the presence of aniline and **H-AzoPh**. In contrast, the characteristic peaks of **O-AzoPh** were not observed in the post-electrolyte solution. As shown in Figure 4a, the **H-AzoPh** species is presumably derived from disproportionation of the proton-assisted one-electron reduction product (intermediate **A** in Figure 4a). Alternatively, the **AzoPh** radical anion (intermediate **B** in Figure 4a) may undergo disproportionation reaction to generate **AzoPh** dianion and **AzoPh**. The **AzoPh** dianion can be protonated to form **H-AzoPh** (Figure 4a).[36] In addition, decomposition could occur by heterolytic cleavage of the N–N bond in the presence of water and generate a N-hydroxyl aniline radical (intermediate **C** in Figure 4a) and aniline anion (intermediate **D** in Figure 4a).[37] Intermediate **D** is protonated to generate aniline (Figure 4a).[36b,37–38] The peaks at 7.35–7.45 ppm is not assigned.

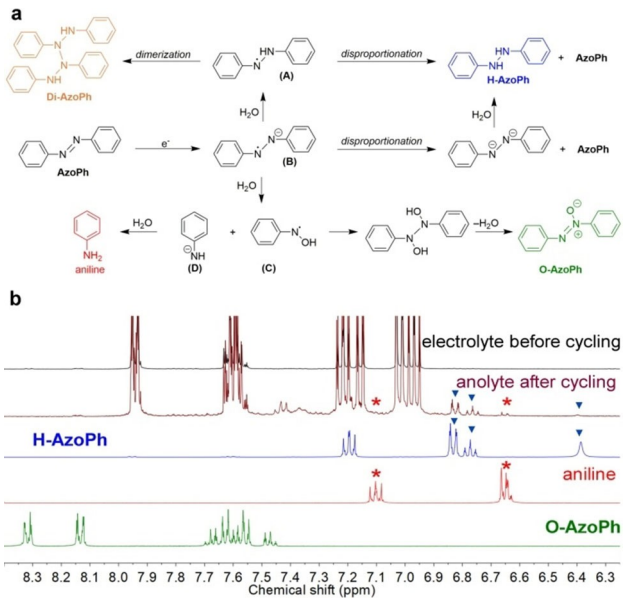


**Figure 4.** a) Proposed decomposition mechanisms of **AzoPh**. b) $^1$H NMR of electrolyte before cycling, anolyte after 80 cycles, and authentic aniline and **H-AzoPh.**

CV test before and after cycling is also an effective way to analyze the cause of battery decay. As shown in Figure 3g, almost identical CV curves of anolyte and catholyte were observed after cycling due to the poor selective permeability of Daramic® 175 membrane. An anodic peak of **H-AzoPh** at 0.25 V vs. Ag/Ag$^+$ was observed in post-cycling anolyte (Figure S8), further confirming the existence of **H-AzoPh** in the post-cycling electrolytes. The CV features of aniline in the post cycling electrolyte are not prominent due to its small amount, as evidenced by $^1$H NMR and the overlapped peaks with **PEG3-PTZ** in the region of 0.5–0.6 V vs. Ag/Ag$^+$. The redox peak of aniline overlaps with that of the electrolytes, thus was not observed. The absence of **O-AzoPh** redox peaks in the post-electrolyte solution also excludes the presence of **O-AzoPh**. HR-MS of the post-cycling electrolyte shows the presence of **H-AzoPh** and aniline, which is consistent with the findings from $^1$H NMR and CV. In addition, the HR-MS results also indicate the formation of the hypothesized azobenzene dimer (**Di-AzoPh**) (Figure 4a and Figure S9).

To further investigate the electrochemical stability of **AzoPh** in the TBAPF$_6$/MeCN system, a series of CV measurements with different cut-off potentials were performed (Figure S10). The redox reaction of **AzoPh** is stable and consistent within a potential ranging from −2.0 to −1.0 V vs. Ag/Ag$^+$. At a wider potential range (−2.0 to 0.2 V vs. Ag/Ag$^+$), no additional redox peaks are found, indicating that the high stability of **AzoPh**. However, the redox peak intensity decreased significantly after 500 cycles, indicating decreased concentration of active species. More severe current decrease was observed when the positive cutoff potential is extended to 0.8 V vs. Ag/Ag$^+$, and the redox features disappeared after 25 CV cycles. The anodic and cathodic currents at −2.20 V vs. Ag/Ag$^+$ for two-electron activity decreased by 26% and 38% over 250 and 500 cycles, respectively. Compared with the reduction reaction under extreme negative voltage, **AzoPh** presents greater extent of destruction under positive voltage.

### 2.4. Two-Electron Redox Activity of AzoPh

An **AzoPh/PEG3-PTZ** RFB with 100-mM **AzoPh** and 200-mM **PEG3-PTZ** was assembled to demonstrate two-electron utilization for higher energy density. The cut-off voltage was set to 3.65 V for charging to achieve the two-electron activity of **AzoPh** (Figure S11). Two charge plateaus at 2.2 V and 3.0 V were observed, corresponding to the two one-electron redox activity of **AzoPh** at −1.69 and −2.20 V vs. Ag/Ag$^+$, respectively. In addition, the battery also delivered a charge capacity of 79.0 mAh, which is slightly higher than the theoretical capacity (64.3 mAh) due to the crossover. However, the high-voltage plateau was not observed in the discharge process, consistent with the instability result from CV measurements. When the azo group is reduced to dianion, the π-electron conjugated system of the two phenyl units is destructed. A large variation in the

electron density and dipole moment in the benzene rings and their substitute groups are expected, which may cause redox reversibility of **AzoPh**.[38–39]

The post-electrolyte solution was analyzed by $^1$H NMR and CV to examine the possible degradation mechanism of the two-electron reaction (Figures S12 and S13). Quantification analysis on the $^1$H NMR indicates 20% of **AzoPh** was converted to **H-AzoPh**, compared to a conversion yield of 7% in the single-electron battery test. The fast kinetics suggest that the doubly reduced species **AzoPh**$^{2-}$ is more vulnerable to protonation to afford **H-AzoPh** than the singly reduced species **AzoPh**$^{-}$. The generated by-product **H-AzoPh** resulted in severe charge between the anolyte and catholyte, causing poor cyclability. On the other hand, the characteristic peak of aniline is still found, albeit weak, in the electrolyte after cycling (Figure S14). Surprisingly, the unidentified peak at 7.35–7.45 ppm in the single-electron reaction was not observed. The CV features of the anolyte and catholyte are retained presumably due to the limited cycles (Figure S15).

### 2.5. Battery Performance at Higher Concentration

In addition, increased concentration accelerates the production of side products: after 14 cycles (70.5 minutes), 16% of **AzoPh** was converted to **H-AzoPh**. Cyclic voltammetry of the post-electrolyte solution indicates the presence of the side products (Figure S11). In addition, we assembled a higher concentration (0.5 M) **AzoPh** based battery, with the intention to explore the stability of **AzoPh** as RFB electrode material in high-concentration batteries. The battery was tested for constant current charging and discharging at a current density of 20 mA/cm$^2$. The capacity retention of the battery was 98.45% per cycle, and 69% for the entire 20 cycles (Figure 5). The results of the post-electrolyte are similar to the previous 100-mM batteries. By-products such as **H-AzoPh** and aniline were found to be generated during the cycle (Figures S11 and S12).

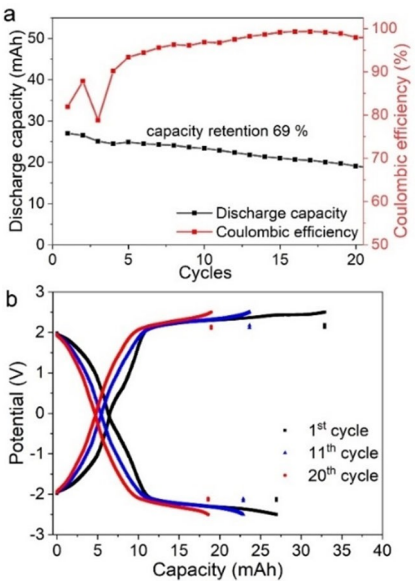


**Figure 5.** a) Discharge capacity and Coulombic efficiency of the 0.5-M **AzoPh** Static symmetrical battery at 20 mA/cm$^2$. b) Charge/discharge profiles at different cycle numbers.

## 3. Conclusions

In summary, we report a new class of electro-active materials, azobenzene and its derivative, as anolyte in organic redox flow batteries. Compound **AzoPh** presents two-electron activity and fast redox kinetics. Paired with **PEG3-PTZ**, the **AzoPh**-based battery delivers a high voltage of 2.08 V and a reversible capacity of 17.8 mAh at a current density of 40 mA/cm$^2$ with a capacity retention of 93.3% over 50 cycles. $^1$H NMR, CV, and HR-MS analysis of the post-cycling electrolyte elucidated the decay mechanism of **AzoPh** and revealed the proton-assisted side reactions with **H-AzoPh** and aniline as the main products. As a new family of anolyte material, azo compounds show their potential for application in high-voltage nonaqueous redox flow batteries.

## Experimental Section

### Chemicals and Manipulations

All chemicals were purchased from Sigma-Aldrich, stored in an argon-filled glovebox, and used as received. The $^1$H NMR analysis was performed at room temperature on a Bruker AV 400 MHz spectrometer. HR-MS analysis was performed on an Orbitrap Fusion Lumos mass spectrometer from Thermo Scientific.

### Battery Measurements

The flow battery is composed of two aluminum alloy plates, two polytetrafluoroethylene plates, two copper plates, two graphite current collectors, two polytetrafluoroethylene frames, and two graphite felt electrodes with an active area of 28 cm$^2$. Daramic®175 membrane was sandwiched between two graphite felts without pretreatment. All battery measurements were conducted using a Bio-Logic potentiostat. For symmetric full RFB for single electron utilization, a mixed electrolyte of 100 mM **AzoPh** and 100 mM **PEG3-PTZ** in 0.5 M TBAPF$_6$/MeCN is used as both anolyte and catholyte. For symmetric full RFB for two electron utilization, 100 mM **AzoPh** and 200 mM **PEG3-PTZ** in 0.5 M TBAPF$_6$/MeCN are used both anolyte and catholyte, respectively. The battery was galvanostatically charged to 2.5 V or 3.65 V. The rate property of full battery was tested under varied current densities using the galvanostatic charge and discharge technique. For static symmetrical full cell, 0.5 M **AzoPh** and **PEG3-PTZ** in 0.5 M TBAPF$_6$/MeCN (6 mL) was used as anolyte and catholyte, respectively. Polarization of full battery at different SOCs were tested following steps below: The battery was charged and discharged at a current density of 40 mA/cm$^2$ for 3 cycles initially, followed by charging to the desired SOC and then polarized by linear sweep voltammetry (LSV) at a scan rate of 100 mV/s and a potential range of 1.2–2.5 V. The impendence of the battery was conducted via electrochemical impedance spectroscopy (EIS) with a frequency ranging from 100 mHz to 200 Hz. The $^1$H NMR analysis of per- and post-electrolyte was performed by diluting the electrolyte with $CD_3CN$ to 50 mM.

**Compound PEG3-PTZ**

A sample of NaH (17.5 g, 729 mmol, 8.30 eq) was added to the solution of phenothiazine (**PTZ**) (17.5 g, 87.8 mmol, 1.00 eq) in DMF (70.0 mL) and stirred at room temperature for 1 hour. PEG3-OTs[40] (22.3 g, 70.2 mmol, 0.800 eq) was added and the resultant mixture was stirred at room temperature for 36 hours. Water was added dropwise to the residue. The mixture was washed three times with brine and extracted with ethyl acetate to remove DMF. The organic extract was combined and dried over $Na_2SO_4$. The solution was filtered, and the filtrate was dried via a rotatory evaporator. The crude residue was purified by column chromatography ($SiO_2$; hexane, $CH_2Cl_2$, and 5–10% MeOH in $CH_2Cl_2$) to afford the title compound as light red oil. Yield: 22.8 g, 75%. $^1$H NMR (400 MHz, $CDCl_3$), δ 3.39 (s, 3H), 3.52–3.58 (m, 2H), 3.61–3.70 (m, 6H), 3.83–3.90 (t, 2H, $J$ = 8.0 Hz), 4.08–4.15 (t, 2H, $J$ = 8.0 Hz), 6.88–6.96 (m, 4H), 7.10–7.19 (m, 4H).

## Acknowledgements

*The authors acknowledge the University of Cincinnati for startup funding support. NMR experiments were performed on a Bruker AVANCE NEO 400 MHz NMR spectrometer funded by NSF-MRI grant CHE-1726092.*

## Conflict of Interest

The authors declare no conflict of interest.

**Keywords:** anolyte · azo compounds · redox flow batteries · nonaqueous · NMR spectroscopy

[1] a) P. Han, G. Xu, X. Han, J. Zhao, X. Zhou, G. Cui, *Adv. Energy Mater.* **2018**, *8*, 1801243; b) M. Sathiya, J. B. Leriche, E. Salager, D. Gourier, J. M. Tarascon, H. Vezin, *Nat. Commun.* **2015**, *6*, 6276; c) G. Wang, L. Zhang, J. Zhang, *Chem. Soc. Rev.* **2012**, *41*, 797; d) G. Xu, X. Shangguan, S. Dong, X. Zhou, G. Cui, *Angew. Chem. Int. Ed.* **2020**, *59*, 3400; e) H. Pan, Y. Shao, P. Yan, Y. Cheng, K. S. Han, Z. Nie, C. Wang, J. Yang, X. Li, P. Bhattacharya, *Nat. Energy* **2016**, *1*, 16039; f) Q. Fan, W. Liu, Z. Weng, Y. Sun, H. Wang, *J. Am. Chem. Soc.* **2015**, *137*, 12946; g) H. Wang, L.-F. Cui, Y. Yang, H. Sanchez Casalongue, J. T. Robinson, Y. Liang, Y. Cui, H. Dai, *J. Am. Chem. Soc.* **2010**, *132*, 13978–13980; h) H. Wang, Y. Yang, Y. Liang, J. T. Robinson, Y. Li, A. Jackson, Y. Cui, H. Dai, *Nano Lett.* **2011**, *11*, 2644–2647.

[2] a) G. L. Soloveichik, *Chem. Rev.* **2015**, *115*, 11533; b) Y. Ding, Y. Zhao, Y. Li, J. B. Goodenough, G. Yu, *Energy Environ. Sci.* **2017**, *10*, 491; c) B. Huskinson, M. P. Marshak, C. Suh, S. Er, M. R. Gerhardt, C. J. Galvin, X. Chen, A. Aspuru-Guzik, R. G. Gordon, M. J. Aziz, *Nature* **2014**, *505*, 195; d) T. Janoschka, N. Martin, U. Martin, C. Friebe, S. Morgenstern, H. Hiller, M. D. Hager, U. S. Schubert, *Nature* **2015**, *527*, 78; e) Z. Yuan, H. Zhang, X. Li, *Chem. Commun.* **2018**, *54*, 7570; f) E. C. Montoto, G. Nagarjuna, J. S. Moore, J. Rodríguez-López, *J. Electrochem. Soc.* **2017**, *164*, A1688.

[3] a) A. Hollas, X. Wei, V. Murugesan, Z. Nie, B. Li, D. Reed, J. Liu, V. Sprenkle, W. Wang, *Nat. Energy* **2018**, *3*, 508; b) J. D. Milshtein, J. L. Barton, T. J. Carney, J. A. Kowalski, R. M. Darling, F. R. Brushett, *J. Electrochem. Soc.* **2017**, *164*, A2487.

[4] a) Y. Liu, M. A. Goulet, L. Tong, Y. Liu, Y. Ji, L. Wu, R. G. Gordon, M. J. Aziz, Z. Yang, T. Xu, *Chem* **2019**, *5*, 1861; b) B. Hu, Y. Tang, J. Luo, G. Grove, Y. Guo, T. L. Liu, *Chem. Commun.* **2018**, *54*, 6871.

[5] a) K. Lin, Q. Chen, M. R. Gerhardt, L. Tong, S. B. Kim, L. Eisenach, A. W. Valle, D. Hardee, R. G. Gordon, M. J. Aziz, *Science* **2015**, *349*, 1529; b) M. Park, J. Ryu, W. Wang, J. Cho, *Nat. Rev. Mater.* **2016**, *2*, 16080.

[6] J. Luo, B. Hu, M. Hu, Y. Zhao, T. L. Liu, *ACS Energy Lett.* **2019**, *4*, 2220.

[7] a) Y. Ding, C. Zhang, L. Zhang, Y. Zhou, G. Yu, *Chem. Soc. Rev.* **2018**, *47*, 69; b) M. Skyllas-Kazacos, M. H. Chakrabarti, S. A. Hajimolana, F. S. Mjalli, M. Saleem, *J. Electrochem. Soc.* **2011**, *158*, R55.

[8] a) R. Chen, *ChemElectroChem* **2018**, *6*, 603; b) A. Tatlisu, Z. Huang, R. Chen, *ChemSusChem* **2018**, *11*, 3899.

[9] W. Wang, W. Xu, L. Cosimbescu, D. Choi, L. Li, Z. Yang, *Chem. Commun.* **2012**, *48*, 6669.

[10] J. Zhang, Z. Yang, I. A. Shkrob, R. S. Assary, S. o. Tung, B. Silcox, W. Duan, J. Zhang, C. C. Su, B. Hu, B. Pan, C. Liao, Z. Zhang, W. Wang, L. A. Curtiss, L. T. Thompson, X. Wei, L. Zhang, *Adv. Energy Mater.* **2017**, *7*, 1701272.

[11] a) J. A. Kowalski, M. D. Casselman, A. P. Kaur, J. D. Milshtein, C. F. Elliott, S. Modekrutti, N. H. Attanayake, N. Zhang, S. R. Parkin, C. Risko, F. R. Brushett, S. A. Odom, *J. Mater. Chem. A* **2017**, *5*, 24371; b) K. Gong, Q. Fang, S. Gu, S. F. Y. Li, Y. Yan, *Energy Environ. Sci.* **2015**, *8*, 3515; c) G. Nagarjuna, J. Hui, K. J. Cheng, T. Lichtenstein, M. Shen, J. S. Moore, J. Rodríguez-López, *J. Am. Chem. Soc.* **2014**, *136*, 16309.

[12] a) C. S. Sevov, S. K. Samaroo, M. S. Sanford, *Adv. Energy Mater.* **2017**, *7*, 1602027; b) N. H. Attanayake, J. A. Kowalski, K. V. Greco, M. D. Casselman, J. D. Milshtein, S. J. Chapman, S. R. Parkin, F. R. Brushett, S. A. Odom, *Chem. Mater.* **2019**, *31*, 4353.

[13] X. Wei, W. Xu, M. Vijayakumar, L. Cosimbescu, T. Liu, V. Sprenkle, W. Wang, *Adv. Mater.* **2014**, *26*, 7649.

[14] J. D. Milshtein, A. P. Kaur, M. D. Casselman, J. A. Kowalski, S. Modekrutti, P. L. Zhang, N. Harsha Attanayake, C. F. Elliott, S. R. Parkin, C. Risko, F. R. Brushett, S. A. Odom, *Energy Environ. Sci.* **2016**, *9*, 3531.

[15] a) S. Jin, E. M. Fell, L. Vina-Lopez, Y. Jing, P. W. Michalak, R. G. Gordon, M. J. Aziz, *Adv. Energy Mater.* **2020**, DOI: 10.1002/aenm.2020001002000100; b) Y. Liu, Y. Li, P. Zuo, Q. Chen, G. Tang, P. Sun, Z. Yang, T. Xu, *ChemSusChem* **2020**, *13*, 2245; c) B. Hu, T. L. Liu, *J. Energy Chem.* **2018**, *27*, 1326.

[16] a) K. H. Hendriks, C. S. Sevov, M. E. Cook, M. S. Sanford, *ACS Energy Lett.* **2017**, *2*, 2430; b) C. S. Sevov, R. E. Brooner, E. Chenard, R. S. Assary, J. S. Moore, J. Rodríguez-López, M. S. Sanford, *J. Am. Chem. Soc.* **2015**, *137*, 14465; c) C. S. Sevov, D. P. Hickey, M. E. Cook, S. G. Robinson, S. Barnett, S. D. Minteer, M. S. Sigman, M. S. Sanford, *J. Am. Chem. Soc.* **2017**, *139*, 2924.

[17] X. Wei, W. Xu, J. Huang, L. Zhang, E. Walter, C. Lawrence, M. Vijayakumar, W. A. Henderson, T. Liu, L. Cosimbescu, B. Li, V. Sprenkle, W. Wang, *Angew. Chem. Int. Ed.* **2015**, *54*, 8684.

[18] J. Huang, Z. Yang, M. Vijayakumar, W. Duan, A. Hollas, B. Pan, W. Wang, X. Wei, L. Zhang, *Adv. Sustainable Syst.* **2018**, *2*, 1700131.

[19] a) G. Wang, B. Huang, D. Liu, D. Zheng, J. Harris, J. Xue, D. Qu, *J. Mater. Chem. A* **2018**, *6*, 13286; b) G. Nagarjuna, J. Hui, K. J. Cheng, T. Lichtenstein, M. Shen, J. S. Moore, J. Rodríguez-López, *J. Am. Chem. Soc.* **2014**, *136*, 16309; c) X. Wei, W. Duan, J. Huang, L. Zhang, B. Li, D. Reed, W. Xu, V. Sprenkle, W. Wang, *ACS Energy Lett.* **2016**, *1*, 705; d) E. C. Montoto, G. Nagarjuna, J. Hui, M. Burgess, N. M. Sekerak, K. Hernandez-Burgos, T. S. Wei, M. Kneer, J. Grolman, K. J. Cheng, J. A. Lewis, J. S. Moore, J. Rodríguez-López, *J. Am. Chem. Soc.* **2016**, *138*, 13230.

[20] a) A. A. Beharry, G. A. Woolley, *Chem. Soc. Rev.* **2011**, *40*, 4422; b) G. S. Kumar, D. Neckers, *Chem. Rev.* **1989**, *89*, 1915; c) S. K. Yesodha, C. K. S. Pillai, N. Tsutsumi, *Prog. Polym. Sci.* **2004**, *29*, 45.

[21] a) Y. Liang, C. Luo, F. Wang, S. Hou, S.-C. Liou, T. Qing, Q. Li, J. Zheng, C. Cui, C. Wang, *Adv. Energy Mater.* **2019**, *9*, 1802986; b) C. Luo, X. Ji, J. Chen, K. J. Gaskell, X. He, Y. Liang, J. Jiang, C. Wang, *Angew. Chem. Int. Ed.* **2018**, *57*, 8567; c) C. Luo, G. L. Xu, X. Ji, S. Hou, L. Chen, F. Wang, J. Jiang, Z. Chen, Y. Ren, K. Amine, C. Wang, *Angew. Chem. Int. Ed.* **2018**, *57*, 2879; d) C. Luo, O. Borodin, X. Ji, S. Hou, K. J. Gaskell, X. Fan, J. Chen, T. Deng, R. Wang, J. Jiang, C. Wang, *Proc. Natl. Acad. Sci. U. S. A.* **2018**, *115*, 2004.

[22] L. Zhang, Y. Qian, R. Feng, Y. Ding, X. Zu, C. Zhang, X. Guo, W. Wang, G. Yu, *Nat. Commun.* **2020**, *11*, 3843.

[23] X. Deng, M. Hu, X. Wei, W. Wang, K. T. Mueller, Z. Chen, J. Z. Hu, *J. Power Sources* **2016**, *308*, 172.

[24] J. Zhang, J. Huang, L. A. Robertson, R. S. Assary, I. A. Shkrob, L. Zhang, *J. Phys. Chem. C* **2018**, *122*, 8116.

[25] J. M. Saveant, C. Tard, *J. Am. Chem. Soc.* **2014**, *136*, 8907.

[26] a) J. Chai, A. Lashgari, Z. Cao, C. K. Williams, X. Wang, J. Dong, J. J. Jiang, *ACS Appl. Mater. Interfaces* **2020**, *12*, 15262; b) J. Chai, A. Lashgari, X. Wang, C. K. Williams, J. J. Jiang, *J. Mater. Chem. A* **2020**, DOI: 10.1039/D0TA02303EDOI:10.1039/d0ta02303e.

[27] C. DeBruler, B. Hu, J. Moss, X. Liu, J. Luo, Y. Sun, T. L. Liu, *Chem* **2017**, *3*, 961.

[28] N. Gallagher, H. Z. Ye, J. Lopez, Y. Zhu, T. Van Voorhis, Y. Shao-Horn, J. A. Johnson, *Angew. Chem. Int. Ed.* **2019**, *132*, 3980.

[29] K. Lin, R. Gómez Bombarelli, E. S. Beh, L. Tong, Q. Chen, A. Valle, A. Aspuru-Guzik, M. J. Aziz, R. G. Gordon, *Nat. Energy* **2016**, *1*, 16102.
[30] S. O. Tung, S. L. Fisher, N. A. Kotov, L. T. Thompson, *Nat. Commun.* **2018**, *9*, 4193.
[31] W. Duan, J. Huang, J. A. Kowalski, I. A. Shkrob, M. Vijayakumar, E. Walter, B. Pan, Z. Yang, J. D. Milshtein, B. Li, C. Liao, Z. Zhang, W. Wang, J. Liu, J. S. Moore, F. R. Brushett, L. Zhang, X. Wei, *ACS Energy Lett.* **2017**, *2*, 1156c1161.
[32] H. Wang, S. Y. Sayed, E. J. Luber, B. C. Olsen, S. M. Shirurkar, S. Venkatakrishnan, U. M. Tefashe, A. K. Farquhar, E. S. Smotkin, R. L. McCreery, J. M. Buriak, *ACS Nano* **2020**, *14*, 2575.
[33] T. Ma, Z. Pan, L. Miao, C. Chen, M. Han, Z. Shang, J. Chen, *Angew. Chem. Int. Ed.* **2018**, *57*, 3158.
[34] L. Tong, M.-A. Goulet, D. P. Tabor, E. F. Kerr, D. De Porcellinis, E. M. Fell, A. Aspuru-Guzik, R. G. Gordon, M. J. Aziz, *ACS Energy Lett.* **2019**, *4*, 1880.
[35] M. Sanford, A. Shrestha, K. Hendriks, M. Sigman, S. Minteer, *Chem. Eur. J.* **2020**, *26*, 5369.
[36] a) S. Cheng, M. D. Hawley, *J. Org. Chem.* **1985**, *50*, 3388; b) W.-W. Zhang, H.-F. Li, L. Liu, J.-L. Xie, C.-S. Lu, Y. Zhou, X.-M. Ren, Q.-J. Meng, *J. Colloid Interface Sci.* **2003**, *261*, 82.
[37] M. K. Bradley, J. Robinson, D. P. Woodruff, *J. Phys. Chem. C* **2013**, *117*, 12591.
[38] B. Šljukić, C. E. Banks, R. G. Compton, *Phys. Chem. Chem. Phys.* **2004**, *6*, 4034.
[39] J. C. Forti, J. A. Nunes, M. R. V. Lanza, R. Bertazzoli, *J. Appl. Electrochem.* **2007**, *37*, 527.
[40] S. Roy, D. Samanta, P. Kumar, T. K. Maji, *Chem. Commun.* **2018**, *54*, 275.

Manuscript received: August 6, 2020
Revised manuscript received: August 24, 2020
Accepted manuscript online: September 1, 2020

# ARTICLES

**It's got potential**: Azobenzene is proved to be a potential anode material for redox flow batteries. The capacity degradation mechanism of azobenzene-based batteries is also verified by methods such as proton nuclear magnetic resonance spectroscopy, cyclic voltammetry, and high-resolution mass spectrometry.

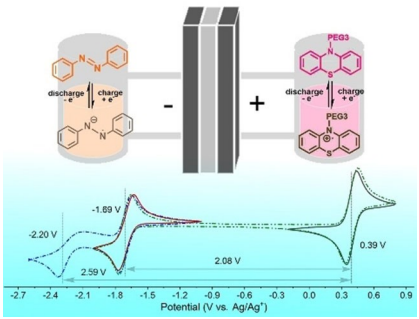


*X. Wang, Dr. J. Chai, Dr. A. Lashgari, Prof. J. J. Jiang**

# Preflight Results

## Document Overview

Title: Azobenzene -Based Low -Potential Anolyte for Nonaqueous Organic Redox Flow Batteries
Author:
Creator: ima-server®
Producer: PDFlib+PDI 9.0.7p3 (C++/Win64); modified using iText 4.2.0 by 1T3XT

## Preflight Information

Profile: Convert to PDF/A-3b
Version: Qoppa jPDFPreflight v2020R2.00
Date: Dec 10, 2020 12:44:24 PM

Legend: (X) - Can NOT be fixed by PDF/A-1b conversion.
(!X) - Could be fixed by PDF/A-1b conversion. User chose to be warned in PDF/A settings.

**Page 1 Results**
(X) Font widths must be the same in both the font dictionary and the embedded font file.
(X) Font widths must be the same in both the font dictionary and the embedded font file.
(X) Font widths must be the same in both the font dictionary and the embedded font file.
(X) Font widths must be the same in both the font dictionary and the embedded font file.
(X) Font widths must be the same in both the font dictionary and the embedded font file.

**Page 2 Results**
(X) Font widths must be the same in both the font dictionary and the embedded font file.
(X) Font widths must be the same in both the font dictionary and the embedded font file.
(X) Font widths must be the same in both the font dictionary and the embedded font file.
(X) Font widths must be the same in both the font dictionary and the embedded font file.
(X) Font widths must be the same in both the font dictionary and the embedded font file.
(X) Font widths must be the same in both the font dictionary and the embedded font file.
(X) Font widths must be the same in both the font dictionary and the embedded font file.
(X) Font widths must be the same in both the font dictionary and the embedded font file.
(X) Font widths must be the same in both the font dictionary and the embedded font file.
(X) Font widths must be the same in both the font dictionary and the embedded font file.
(X) Font widths must be the same in both the font dictionary and the embedded font file.
(X) Font widths must be the same in both the font dictionary and the embedded font file.
(X) Font widths must be the same in both the font dictionary and the embedded font file.

**Page 3 Results**
(X) Font widths must be the same in both the font dictionary and the embedded font file.
(X) Font widths must be the same in both the font dictionary and the embedded font file.
(X) Font widths must be the same in both the font dictionary and the embedded font file.
(X) Font widths must be the same in both the font dictionary and the embedded font file.
(X) Font widths must be the same in both the font dictionary and the embedded font file.
(X) Font widths must be the same in both the font dictionary and the embedded font file.
(X) Font widths must be the same in both the font dictionary and the embedded font file.
(X) Font widths must be the same in both the font dictionary and the embedded font file.
(X) Font widths must be the same in both the font dictionary and the embedded font file.

**Page 4 Results**
(X) Font widths must be the same in both the font dictionary and the embedded font file.
(X) Font widths must be the same in both the font dictionary and the embedded font file.
(X) Font widths must be the same in both the font dictionary and the embedded font file.
(X) Font widths must be the same in both the font dictionary and the embedded font file.
(X) Font widths must be the same in both the font dictionary and the embedded font file.
(X) Font widths must be the same in both the font dictionary and the embedded font file.
(X) Font widths must be the same in both the font dictionary and the embedded font file.

**Page 5 Results**
(X) Font widths must be the same in both the font dictionary and the embedded font file.
(X) Font widths must be the same in both the font dictionary and the embedded font file.